Measurement of the Adsorption at Solid−Liquid Interfaces from the Pressure Dependence of Contact Angles

ARTICLE *in* THE JOURNAL OF PHYSICAL CHEMISTRY B · FEBRUARY 2008

Impact Factor: 3.3 · DOI: 10.1021/jp076195f · Source: PubMed

3 AUTHORS, INCLUDING:

Charles Albert Ward
University of Toronto
141 PUBLICATIONS **2,585** CITATIONS

Measurement of the Adsorption at Solid−Liquid Interfaces from the Pressure Dependence of Contact Angles

C. A. Ward,* Jiyu Wu, and A. Keshavarz

Thermodynamics and Kinetics Laboratory, Department of Mechanical and Industrial Engineering, University of Toronto, Toronto, Canada M5S 3G8

Received: August 2, 2007; In Final Form: October 17, 2007

Earlier studies have indicated that in an isothermal three-phase system, the liquid-phase pressure at the three-phase line, x_3^L, may be viewed as the independent variable of the contact angle, θ, and that adsorption at the solid−liquid interface is the mechanism relating them. When the liquid−vapor interface is axi-symmetric, we show that θ can be predicted as a function of x_3^L and that by measuring $\theta(x_3^L)$, the amount adsorbed at the solid−liquid interface can be determined. We consider water in differently sized borosilicate glass cylinders. For progressively larger cylinders, x_3^L increases with cylinder radius, but when a particularly sized cylinder is rotated about it longitudinal axis, x_3^L is decreased. The observed value of θ in each case is found to be in close agreement with that predicted. A Gibbs model of the interphase is used, and the Gibbs adsorption at the solid−liquid interface is found to be negative. As x_3^L increases above its value at wetting, the amount adsorbed at the solid−liquid interface becomes progressively more negative. Negative adsorption is shown to mean that the concentration of the fluid component is greater in the bulk liquid than in the interphase and that the difference in concentration increases as x_3^L is increased. The data is used to investigate the hypothesis that the curvature of the three-phase line affects θ through line tension, but we find no relation between line tension and θ. There is an apparent relation between the curvature of the liquid−vapor interface, $C^{LV}$and θ, but this is shown to be because C^{LV} affects x_3^L.

1. Introduction

With few exceptions,[1−5] the pressure dependence of the contact angle, θ, on smooth, homogeneous surfaces has been ignored; however, under equilibrium conditions, a difference in contact angles of as much as ∼79° was recently reported when water contacted borosilicate glass in an isothermal system, and the difference in pressure between the three-phase lines was 2.386 cm-H_2O or 235 Pa.[2] For smaller values of the pressure difference, smaller values of the contact-angle difference was observed. Similar results had been observed in other circumstaces,[3,5] but in those previous studies, it could not be claimed with certainty that the system was in equilibrium when the contact angles were recorded. However, in ref 2, an independent criterion for equilibrium was established, and indicated thermodynamic equilibrium had been reached before the contact angles were recorded. For a given system, the experimental results consistently indicate θ increases with pressure at the three-phase line.

The thermodynamic analysis proposed in ref 1 provides a possible explanation for these observations. In that analysis, (1) Gibbsian thermodynamics[6] is supplemented with an adsorption-isotherm expression at the solid−vapor interface (the ζ-isotherm) that is valid when the vapor-phase pressure approaches the saturation vapor pressure; (2) the positions of the solid−vapor and solid−liquid interfaces were chosen so there was no adsorption of the solid component; and (3) the surface tension at the solid−liquid interface was assumed to vanish when θ was zero. If the liquid−vapor interface can be approximated as spherical, as was possible in ref 2, then in an isothermal system, an explicit expression for θ as a function of the liquid-phase pressure evaluated at the three-phase line, x_3^L, was obtained. When the predictions made from this relation were compared with the observations, close agreement was found over a range of pressures.[2]

The reason for the increase in θ with x_3^L is indicated to be the negative adsorption at the solid−liquid interface, $n_{[1]}^{SL}$. Although it is understood that this results from the choice of the solid−liquid interface position,[7,8] we show that negative adsorption at the solid−liquid interface physically means the concentration of the liquid component is higher in the bulk phase than in the interphase. This conclusion is supported by measurements of water density in 14 nm diameter silica−gel pores that have indicated water density to be ∼3% less than its bulk density,[9−11] and in silica glass with pore diameters in the range 3−8 nm, water density is indicated to be 12 to 16% less.[12] Although we deal with a pure fluid, Landau and Lifshitz[13] have shown that, when a solute adsorbs from a solution and the adsorption is negative, the solute accumulates preferentially in the bulk phase, as opposed to in the interphase.

The increase in θ with x_3^L provides a possible explanation for contact angle hysteresis on smooth homogeneous surfaces.[1−5,14] The usual explanation for contact angle hysteresis of a sessile droplet is roughness or heterogeneity underneath the droplet.[15−18] Although this approach had been questioned earlier,[19] Gao and McCarthy[20] recently gave convincing evidence that it is the condition at the three-phase line that determines contact-angle hysteresis. The results reported by Gao and McCarthy are consistent with the suggestion that it is adsorption at the three-phase line and its dependence on x_3^L that is responsible.

* Corresponding author. E-mail: ward@mie.utoronto.ca.

10.1021/jp076195f CCC: $40.75
Published on Web 12/11/2007

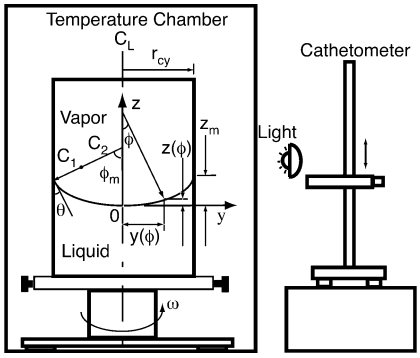

Figure 1. Schematic of the apparatus used to observe the contact angle dependence on pressure and temperature in both the static and the rotating experiments. When the rotating experiments were performed, the rotation was about the longitudinal axis of the cylinder.

In general, a sessile droplet cannot be approximated as having a spherical liquid−vapor interface. We remove this assumption. For axisymmetric liquid−vapor interfaces, Gibbsian thermodynamics indicates θ increases with x_3^L (as it does for a spherical liquid−vapor interface). This prediction is examined by two independent experimental techniques. Both the contact angle and the value of x_3^L when water and its vapor are held in a series of progressively larger diameter glass cylinders were determined from the measurement of the meniscus height. For cylinders of progressively larger diameter, both θ and x_3^L progressively increase. In a separate set of experiments, x_3^L was reduced by rotating the cylinders about their longitudinal axes, and θ was observed to be reduced with increasing rotation rate. The theoretical $\theta(x_3^L)$ relation is used to establish the adsorption isotherms at the solid−liquid interface, and the measured relation between $\theta(x_3^L)$ is used to determine the amount adsorbed at the solid−liquid interface. The predictions and the measurements agree closely.

Good and Koo[21] pointed out that a number of experimental studies had indicated θ depended on the radius of the three-phase contact line: the "droplet-size effect". They investigated the possibility that line tension was responsible and found that if it were, then line tension had to be negative. Good felt a negative line tension was "physically unreasonable",[22] but a number of subsequent studies (e.g., refs 23−27) investigated the possibility of line tension being responsible for the droplet-size effect. These studies have not led to a consistent magnitude nor a consistent sign of the line tension. Our data indicates to the contrary: θ is independent of the three-phase line curvature. One thing that all of the previous line tension studies have in common is that they neglected the adsorption at the solid−liquid interface. We show that if adsorption there is taken into account the curvature of the liquid−vapor interface, through its effect on x_3^L, can strongly change the contact angle.

2. Contact Angle Dependence on the Pressure at the Three-Phase Line

Consider a liquid and its vapor of molecular weight W held in a container that has a smooth homogeneous surface, is maintained at temperature T, and is exposed to gravitational and centrifugal fields. Suppose that, at the three-phase line, a contact angle θ is formed (Figure 1). One of the conditions for thermodynamic equilibrium is the Young equation.[4] It relates the surface tensions at the solid−vapor, solid−liquid, and liquid−vapor interfaces, $\gamma_{[1]}^{SV}$, $\gamma_{[1]}^{SL}$, and γ^{LV} respectively, to θ:

$$\gamma_{[1]}^{SV} - \gamma_{[1]}^{SL} = \gamma^{LV}\cos\theta \tag{1}$$

where the bracketed subscript indicates the positions of the interfaces at the solid−vapor and solid−liquid interfaces are chosen such that there is no adsorption of the solid component. If the chemical potential in phase j is denoted as μ^j, the potential energy per unit mass as ξ, a second condition for equilibrium may be written[28,29]

$$\mu^j + W\xi = \lambda \qquad j = L, V, LV, SV, \text{or } SL \tag{2}$$

where λ is a constant. For a system exposed to a gravitational field of intensity g and to a centrifugal field corresponding to an angular speed of ω, at a height z and radial position y, ξ may be written

$$\xi = gz - \frac{\omega^2 y^2}{2} \tag{3}$$

When eq 2 is applied at a position on a liquid−vapor interface, z and y have the same values in each phase; thus

$$\mu^L = \mu^V \tag{4}$$

If the molar specific volume of the liquid at saturation is denoted as v_f, the saturation vapor pressure as $P_s(T)$, the ratio of the liquid-phase pressure to the saturation vapor pressure as $x^L(y, z)$, and the isothermal compressibility as κ_T, then provided $|\kappa_T P_s[x^L(y, z) - 1]| \ll 1$, the chemical potential in the liquid may be expressed

$$\mu^L[T, x^L(y, z)] = \mu(T, P_s) + v_f P_s[x^L(y, z) - 1] \tag{5}$$

If the vapor phase is approximated as an ideal gas:

$$\mu^V[T, x^V(y, z)] = \mu(T, P_s) + k_b T \ln[x^V(y, z)] \tag{6}$$

where k_b is the Boltzmann constant. If a position on the liquid−vapor interface is denoted r_I, then after substituting eqs 5 and 6 into eq 4

$$x^V(r_I) = \exp\left(\frac{v_f}{v_g}[x^L(r_I) - 1]\right) \tag{7}$$

where v_g is the specific volume of the vapor phase at saturation. Thus, if the pressure is such that θ can exist, then $x^L(r_I)$ may be viewed as the independent variable of the two pressures at the liquid−vapor interface. If at the three-phase line $x^L(y_3, z_3)$ is unity, then $x^V(y_3, z_3)$ is as well. This condition would exist if θ were equal to $\pi/2$.

The Gibbs−Duhem equation gives

$$\mathrm{d}\mu^L = -s^L\,\mathrm{d}T + v_f P_s\,\mathrm{d}x^L \tag{8}$$

If the amounts adsorbed at the solid−vapor and solid−liquid interfaces approaching the three-phase line from within the vapor and from within the liquid phases are denoted $n_{[1]}^{SV}(x_3^L)$ and $n_{[1]}^{SL}(x_3^L)$, respectively, then, for an isothermal system, the Gibbs adsorption equation at the solid−vapor interface may be written

$$\mathrm{d}\gamma_{[1]}^{SV}(x_3^L) = -n_{[1]}^{SV}(x_3^L)v_f P_s\,\mathrm{d}x_3^L \tag{9}$$

and at the solid−liquid interface:

$$\mathrm{d}\gamma_{[1]}^{SL}(x_3^L) = -n_{[1]}^{SL}(x_3^L)v_f P_s\,\mathrm{d}x_3^L \tag{10}$$

Equations 9 and 10 indicate that $\gamma_{[1]}^{SV}$ and $\gamma_{[1]}^{SL}$ have as their independent variable x_3^L. By differentiating the Young equa-

tion, eq 1, and substituting eqs 9 and 10 into the result, one obtains

$$\frac{\mathrm{d}\cos\theta(x_3^L)}{\mathrm{d}x_3^L} = \left(\frac{v_f P_s}{\gamma^{LV}}\right)[n_{[1]}^{SL}(x_3^L) - n_{[1]}^{SV}(x_3^L)] \tag{11}$$

therefore,

$$\theta = \theta(x_3^L) \tag{12}$$

and the net adsorption, $n_{[1]}^{SL}(x_3^L) - n_{[1]}^{SV}(x_3^L)$ is indicated to be the mechanism that relates θ with x_3^L.

The contact angle can only exist in a limited pressure range.[1] If x_w^L denotes the liquid-phase pressure ratio at the three-phase line when θ is zero and x_π^L the value of this ratio when θ is π, then the range of pressures where θ can exist is defined as $x_w^L \le x_3^L \le x_\pi^L$.

If the adsorbate at the solid−vapor interface is approximated as a collection of molecular clusters with a maximum of one cluster possibly adsorbed at one of the M adsorption sites on a smooth homogeneous, solid surface and each cluster is allowed a maximum of ζ molecules, then an expression for an adsorption isotherm (called the ζ-isotherm) can be obtained by applying statistical thermodynamics.[1] This isotherm contains four parameters (M, c, α, and ζ) that can be determined from adsorption measurements made for a particular vapor−solid system. The isotherm expression may be simplified without losing accuracy if ζ is allowed to approach infinity. If this simplification is made, the result substituted into eq 9, and the modified eq 9 integrated, one finds

$$\gamma_{[1]}^{SV}(x^V) = \gamma^{LV} + Mk_bT\ln\left[\frac{(1-\alpha x^V)(1+(c-1)\alpha x_w^V)}{(1-\alpha x_w^V)(1+(c-1)\alpha x^V)}\right] \tag{13}$$

The ζ-isotherm has the essential property of *not* indicating an infinite amount adsorbed when x^V approaches unity. This transition occurs when x^V approaches $1/\alpha$. It was shown in ref 1 that the ζ-isotherm gave a good description of the adsorption properties of five different vapor−solid systems that had previously been reported in the literature, and α was less than unity for each of them. Thus, the vapor must be supersaturated before condensation occurs.

The surface tension of the solid surface in the absence of adsorption, γ^{S0}, can be expressed in terms of the adsorption parameters. Even though x_w^L deviates by up to 30% from unity, x_w^V is indicated by eq 7 to be very near unity. After approximating x_w^V as unity and evaluating eq 13 at x^V equal zero, one finds

$$\gamma_{[1]}^{S0} = \gamma^{LV} + Mk_bT\ln\left(1+\frac{c\alpha}{1-\alpha}\right) \tag{14}$$

We emphasize that θ cannot exist when x^V is equal to zero. The expression for γ^{S0} given in eq 14 was examined experimentally in ref 1 and shown to be independent of the vapor used to determine its value.

In the pressure range where θ can exist, it was found that the second term in eq 13 was negligible compared with the first for each of the systems considered, and one was H_2O−silica. Thus, when θ can exist for the system, we consider

$$\gamma_{[1]}^{SV}(x_3^L) = \gamma^{LV} \tag{15}$$

and

$$\gamma_{[1]}^{SL}(x_3^L) = \gamma_{[1]}^{SV}(x_3^L)[1-\cos\theta(x_3^L)] \tag{16}$$

The existence of relations such as those in eqs 15 and 16 had been forecast some time ago,[30] but these relations could not be explicitly formulated until an adsorption isotherm was available that could be applied when the vapor-phase pressure was near the saturation vapor pressure. The ζ-isotherm appears to be the required isotherm relation.[1,2]

The availability of eqs 15 and 16 makes it possible to determine the adsorption as a function of x_3^L. As indicated by eq 15, $\gamma_{[1]}^{SV}(x_3^L)$ is constant for the range of pressures where θ can exist. Thus, differentiating eq 16 gives

$$\frac{\mathrm{d}\gamma_{[1]}^{SL}}{\mathrm{d}x_3^L} = \frac{\gamma^{LV}\sin\theta(x_3^L)\,\mathrm{d}\theta(x_3^L)}{\mathrm{d}x_3^L} \tag{17}$$

And after combining eq 17 with eq 10:

$$n_{[1]}^{SL} = -\frac{\gamma^{LV}\sin\theta(x_3^L)}{v_f P_s}\frac{\mathrm{d}\theta(x_3^L)}{\mathrm{d}x_3^L} \tag{18}$$

By establishing the function $\theta(x_3^L)$ experimentally, the value of $n_{[1]}^{SL}(x_3^L)$ can be determined from eq 18. We consider two experimental methods for establishing the relation between θ and x_3^L.

3. Experimental Methodology

Nine right-circular-borosilicate (Pyrex 7740) glass cylinders were partially filled with reagent grade I water (IRG) and used in the stationary experiments. Eight of the cylinders were also used in the rotational experiments. The inside diameter of each cylinder was determined from a glass ring cut from the same glass tube that was used to make the cylinder. The inside diameter of each ring was measured with vernier calipers at 120° intervals around the ring circumference, and the means and standard deviations were calculated. The values are listed in Table 1.

A 15 cm length of a 3.5 mm inside-diameter capillary was attached to the side of each cylinder. The axis of the capillary was perpendicular to the longitudinal cylinder axis. It was used to partially fill each cylinder with water and for degassing the water. After the capillary had been attached, the cylinder−capillary system was annealed at 575 °C.

The water used in the experiments was demineralized, distilled, and nanofiltered using a system designed to produce regent grade I water (IRG). The resistivity of the water at the outlet of the preparation system was 18.2 MΩ cm, and the average surface tension was within 0.3% of the documented value corresponding to the temperature.

In the cleaning procedure, the glass cylinder and attached capillary were first rinsed with acetone then with IRG water before being soaked in a detergent (Alconox) solution for 24 h. After rinsing with IRG water again, they were soaked in a solution of chromic and sulfuric acid for another 24 h before a final rinsing with IRG water.

Samples of IRG water were degassed in separately cleaned glass cylinders. Each cylinder was attached to a vacuum system. Degassed water was added to a degassing vessel through the attached capillary, using a vacuum filling procedure that ensured the liquid was in contact only with cleaned glass or cleaned polytetrafluoroethylene. There was minimal exposure to air.

Each cylinder−capillary system was partially filled with water and placed in a microwave oven, where it was heated until the

TABLE 1: Summary of Results of Stationary Experiments

cylinder radius r_{cy} (mm)	1.75 (±0.01)	4.00 (±0.01)	8.20 (±0.01)	12.06 (±0.01)	24.80 (±0.01)	32.95 (±0.01)	37.84 (±0.01)	42.84 (±0.01)	48.29 (±0.01)
(5 ± 0.1) °C									
$z(\phi_m)$ (mm)	1.47	2.64	3.51	3.62	3.53	3.46	3.40	3.33	3.24
	(±0.03)	(±0.03)	(±0.03)	(±0.03)	(±0.03)	(±0.03)	(±0.03)	(±0.03)	(±0.03)
$x^L(\phi_m)$	0.89186	0.93884	0.95320	0.95725	0.96028	0.96109	0.96177	0.96256	0.96357
	($\pm 9 \times 10^{-4}$)	($\pm 5 \times 10^{-4}$)	($\pm 5 \times 10^{-4}$)	($\pm 4 \times 10^{-4}$)	($\pm 3 \times 10^{-4}$)	($\pm 3 \times 10^{-4}$)	($\pm 3 \times 10^{-4}$)	($\pm 3 \times 10^{-4}$)	($\pm 3 \times 10^{-4}$)
θ (°)	6.0	9.1	11.6	14.2	15.3	16.0	17.0	18.5	20.4
	(±1.5)	(±0.9)	(±0.9)	(±0.7)	(±0.8)	(±0.8)	(±0.8)	(±0.8)	(±0.7)
(10 ± 0.1) °C									
$z(\phi_m)$ (mm)	1.56	2.71	3.57	3.69	3.59	3.52	3.46	3.38	3.30
	(±0.03)	(±0.03)	(±0.03)	(±0.03)	(±0.02)	(±0.02)	(±0.02)	(±0.02)	(±0.02)
$x^L(\phi_m)$	0.92286	0.95618	0.96635	0.96910	0.97131	0.97189	0.97237	0.97301	0.97365
	($\pm 5 \times 10^{-4}$)	($\pm 3 \times 10^{-4}$)	($\pm 3 \times 10^{-4}$)	($\pm 2 \times 10^{-4}$)	($\pm 2 \times 10^{-4}$)	($\pm 2 \times 10^{-4}$)	($\pm 2 \times 10^{-4}$)	($\pm 2 \times 10^{-4}$)	($\pm 2 \times 10^{-4}$)
θ (°)	2.2	6.9	9.8	12.1	13.4	14.0	15.1	16.8	18.5
	(±1.4)	(±0.9)	(±0.8)	(±0.8)	(±0.5)	(±0.5)	(±0.5)	(±0.5)	(±0.5)
(20 ± 0.1) °C									
$z(\phi_m)$ (mm)	1.57	2.76	3.63	3.80	3.68	3.61	3.55	3.45	3.37
	(±0.03)	(±0.03)	(±0.03)	(±0.03)	(±0.02)	(±0.02)	(±0.02)	(±0.02)	(±0.02)
$x^L(\phi_m)$	0.96016	0.97706	0.98219	0.98337	0.98459	0.98489	0.98514	0.98556	0.98589
	($\pm 3 \times 10^{-4}$)	($\pm 2 \times 10^{-4}$)	($\pm 1 \times 10^{-4}$)	($\pm 1 \times 10^{-4}$)	($\pm 1 \times 10^{-4}$)	($\pm 9 \times 10^{-5}$)	($\pm 1 \times 10^{-4}$)	($\pm 1 \times 10^{-4}$)	($\pm 1 \times 10^{-4}$)
θ (°)	1.7	5.1	7.6	8.4	10.1	10.8	11.9	14.2	15.9
	(±1.4)	(±0.9)	(±0.8)	(±0.8)	(±0.8)	(±0.5)	(±0.8)	(±0.8)	(±0.8)
(40 ± 0.1) °C									
$z(\phi_m)$ (mm)	1.59	2.79	3.69	3.85	3.78	3.71	3.65	3.59	3.52
	(±0.03)	(±0.03)	(±0.03)	(±0.03)	(±0.03)	(±0.02)	(±0.02)	(±0.02)	(±0.03)
$x^L(\phi_m)$	0.98785	0.99291	0.99437	0.99472	0.99502	0.99511	0.99519	0.99527	0.99536
	($\pm 8 \times 10^{-5}$)	($\pm 5 \times 10^{-5}$)	($\pm 4 \times 10^{-5}$)	($\pm 4 \times 10^{-5}$)	($\pm 4 \times 10^{-5}$)	($\pm 3 \times 10^{-5}$)	($\pm 3 \times 10^{-5}$)	($\pm 3 \times 10^{-5}$)	($\pm 4 \times 10^{-5}$)
θ (°)	0.7	3.6	4.5	5.2	5.3	6.0	7.2	8.5	10.1
	(+1.4/-0.7)	(±1.0)	(±0.8)	(±0.8)	(±0.6)	(±0.6)	(±0.6)	(±0.6)	(±0.8)
(80 ± 0.1) °C									
$z(\phi_m)$ (mm)	1.61	2.87	3.74	3.89	3.80	3.73	3.68	3.63	3.56
	(±0.03)	(±0.03)	(±0.03)	(±0.03)	(±0.03)	(±0.03)	(±0.02)	(±0.02)	(±0.02)
$x^L(\phi_m)$	0.99828	0.99896	0.99915	0.99920	0.99924	0.99925	0.99926	0.99927	0.99928
	($+8 \times 10^{-6}$)	($+5 \times 10^{-6}$)	($+2 \times 10^{-6}$)	($+2 \times 10^{-6}$)	($+5 \times 10^{-6}$)	($\pm 1 \times 10^{-5}$)	($\pm 4 \times 10^{-6}$)	($\pm 4 \times 10^{-6}$)	($\pm 4 \times 10^{-6}$)
θ (°)	~ 0	~ 0	~ 0	~ 0	~ 0	0.7	1.7	2.8	4.6
	(+0.8/-0)	(+0.6/-0)	(+0.4/-0)	(+0.4/-0)	(+0.8/-0)	(+0.9/-0.7)	(±0.6)	(±0.6)	(±0.6)

water inside the cylinder was boiling. While still boiling, the capillary was connected to a vacuum pump, and the system was evacuated. With the system being evacuated, the capillary was heated with a torch until the capillary was fused closed to completely seal each water sample within a glass cylinder. Thus, the IRG water used in the experiments was fully degassed.

In the stationary experiments, each of the nine glass cylinders that had been partially filled with water were placed separately in an air bath (Thermotron) that was maintained at 5, 10, 20, 40, or 80 ± 0.1 °C. After leveling a partially filled cylinder and allowing it to come to thermal equilibrium, the meniscus height on the longitudinal centerline of each cylinder was measured with a cathetometer placed outside the air bath. This instrument could be read with a precision of 10 μm. The measured meniscus heights of the stationary experiments are listed in Table 1.

In the rotational experiments, each of the eight glass cylinders that had been partially filled with water and used in the stationary experiments were mounted on a rotator (see Figure 1). Each was placed in an air-thermal bath and maintained at 5 ± 0.1 °C. The rotator (a geared motor and controller, Contrex, model ML-Drive) was used to rotate the glass cylinders at frequencies of 0.083, 0.167, or 0.25 Hz. The speed control had a precision of 0.01% of the set speed. A digital stroboscope (Shimpo) was used to check the rotation rate. No significant deviation was observed between the controller and the stroboscope readings. After allowing each system to come to equilibrium, the meniscus height on the centerline of each water−glass cylinder was measured with a cathetometer, and the rotating angular speed was recorded. The results of rotational experiments are listed in Table 2.

4. Functional Relation between x_3^L and θ

Each of the cylinders is assumed to be maintained isothermal while exposed to gravitational and centrifugal fields. A modified turning-angle method[28,31,32] was used to determine the functional relation between x_3^L and θ. The turning angle, ϕ, is indicated in Figure 1.

If the curvatures of the liquid−vapor interface are denoted $C_1^{LV}(\phi)$ and $C_2^{LV}(\phi)$ and are taken to be positive when the vapor is inside the interface, then, after taking advantage of eq 7, the Laplace equation may be written

$$C_1^{LV}(\phi) + C_2^{LV}(\phi) = \frac{P_s}{\gamma^{LV}}\left(\exp\left[\frac{v_f}{v_g}(x^L(\phi) - 1)\right] - x^L(\phi)\right) \quad (19)$$

The curvature $C_2^{LV}(\phi)$ is related to ϕ and the radial position on the interface $y(\phi)$ by

$$C_2^{LV}(\phi) = \frac{\sin\phi}{y(\phi)} \quad (20)$$

On the longitudinal axis of symmetry, C_1^{LV} and C_2^{LV} are equal and are denoted as $C^{LV}(0)$. When applied on this axis, eq 19 reduces to

$$C^{LV}(0) = \frac{P_s}{2\gamma^{LV}}\left(\exp\left[\frac{v_f}{v_g}(x^L(0) - 1)\right] - x^L(0)\right) \quad (21)$$

TABLE 2: Summary of Rotational Experimental Results

cylinder radius r_{cy} (mm)	4.00 (±0.01)	8.20 (±0.01)	12.06 (±0.01)	24.80 (±0.01)	32.95 (±0.01)	37.84 (±0.01)	42.84 (±0.01)	48.29 (±0.01)
ω=0								
$z(\phi_m)$ (mm)	2.64 (±0.03)	3.51 (±0.03)	3.62 (±0.03)	3.53 (±0.03)	3.46 (±0.03)	3.40 (±0.03)	3.33 (±0.03)	3.24 (±0.03)
$x^L(\phi_m)$	0.93884 ($\pm 5 \times 10^{-4}$)	0.95320 ($\pm 5 \times 10^{-4}$)	0.95725 ($\pm 4 \times 10^{-4}$)	0.96028 ($\pm 3 \times 10^{-4}$)	0.96109 ($\pm 3 \times 10^{-4}$)	0.96177 ($\pm 3 \times 10^{-4}$)	0.96256 ($\pm 3 \times 10^{-4}$)	0.96357 ($\pm 3 \times 10^{-4}$)
θ (°)	9.1 (±0.9)	11.6 (±0.9)	14.2 (±0.7)	15.3 (±0.8)	16.0 (±0.8)	17.0 (±0.8)	18.5 (±0.8)	20.4 (±0.7)
ω=0.083 Hz								
$z(\phi_m)$ (mm)	2.67 (±0.025)	3.56 (±0.03)	3.67 (±0.03)	3.57 (±0.03)	3.50 (±0.03)	3.44 (±0.03)	3.36 (±0.03)	3.28 (±0.03)
$x^L(\phi_m)$	0.93845 ($\pm 4 \times 10^{-4}$)	0.95262 ($\pm 4 \times 10^{-4}$)	0.95670 ($\pm 3 \times 10^{-4}$)	0.95992 ($\pm 3 \times 10^{-4}$)	0.96081 ($\pm 3 \times 10^{-4}$)	0.96154 ($\pm 3 \times 10^{-4}$)	0.96250 ($\pm 3 \times 10^{-4}$)	0.96348 ($\pm 3 \times 10^{-4}$)
θ (°)	8.2 (±0.8)	10.4 (±0.8)	13.0 (±0.8)	14.5 (±0.8)	15.3 (±0.8)	16.5 (±0.8)	18.3 (±0.8)	20.2 (±0.7)
ω=0.167 Hz								
$z(\phi_m)$ (mm)	2.70 (±0.03)	3.59 (±0.03)	3.73 (±0.03)	3.64 (±0.03)	3.58 (±0.03)	3.51 (±0.03)	3.45 (±0.03)	3.38 (±0.03)
$x^L(\phi_m)$	0.93806 ($\pm 4 \times 10^{-4}$)	0.95230 ($\pm 4 \times 10^{-4}$)	0.95607 ($\pm 3 \times 10^{-4}$)	0.95941 ($\pm 3 \times 10^{-4}$)	0.96040 ($\pm 3 \times 10^{-4}$)	0.96141 ($\pm 3 \times 10^{-4}$)	0.96234 ($\pm 3 \times 10^{-4}$)	0.96344 ($\pm 3 \times 10^{-4}$)
θ (°)	7.3 (±0.9)	9.6 (±0.8)	11.6 (±0.8)	13.3 (±0.8)	14.3 (±0.8)	16.0 (±0.8)	17.7 (±0.8)	19.9 (±0.8)
ω=0.25 Hz								
$z(\phi_m)$ (mm)	2.73 (±0.03)	3.62 (±0.03)	3.78 (±0.03)	3.70 (±0.03)	3.67 (±0.03)	3.62 (±0.03)	3.58 (±0.03)	3.55 (±0.03)
$x^L(\phi_m)$	0.93769 ($\pm 5 \times 10^{-4}$)	0.95199 ($\pm 4 \times 10^{-4}$)	0.95560 ($\pm 3 \times 10^{-4}$)	0.95919 ($\pm 3 \times 10^{-4}$)	0.96022 ($\pm 3 \times 10^{-4}$)	0.96128 ($\pm 3 \times 10^{-4}$)	0.96230 ($\pm 3 \times 10^{-4}$)	0.96334 ($\pm 3 \times 10^{-4}$)
θ (°)	6.5 (±0.9)	8.9 (±0.8)	10.5 (±0.8)	12.6 (±0.8)	13.6 (±0.8)	15.5 (±0.8)	17.3 (±0.8)	19.3 (±0.8)

After making use of the expression for the chemical potential in the liquid, eq 5, and applying eq 2 at an arbitrary point on the liquid−vapor interface and at the point where the liquid−vapor interface crosses the longitudinal axis of symmetry, one finds

$$x^L(\phi) = x^L(0) - \frac{W}{v_f P_s}\left[gz(\phi) - \frac{\omega^2 y(\phi)^2}{2}\right] \qquad (22)$$

The expression for $C_1(\phi)$ may be obtained from eqs 19−22:

$$C_1^{LV} = \frac{P_s x^V(0)}{\gamma^{LV}}\left(\exp\left[-\frac{W}{P_s v_g}\left(gz(\phi) - \frac{\omega^2 y(\phi)^2}{2}\right)\right] - 1\right) + 2C^{LV}(0) - \frac{\sin\phi}{y(\phi)} + \frac{W}{\gamma^{LV} v_f}\left(gz(\phi) - \frac{\omega^2 y(\phi)^2}{2}\right) \qquad (23)$$

and from differential geometry

$$\frac{dy(\phi)}{d\phi} = \frac{\cos\phi}{C_1^{LV}} \qquad (24)$$

$$\frac{dz(\phi)}{d\phi} = \frac{\sin\phi}{C_1^{LV}} \qquad (25)$$

The contact angle is related to the maximum value of the turning angle, ϕ_m:

$$\theta = \pi/2 \pm \phi_m \qquad (26)$$

where the negative sign is taken if the vapor is inside the surface of curvature. The expression for $x^L(\phi_m)$ may be obtained from eq 22:

$$x^L(\phi_m) = x^L(0) + \frac{W}{v_f P_s}\left[\frac{(\omega r_{cy})^2}{2} - gz(\phi_m)\right] \qquad (27)$$

where r_{cy} is the cylinder radius.

An iterative procedure, employing eqs 21 to 27, may be used to establish the theoretical relation between θ and x_3^L. For given values of r_{cy}, ω, and T, a value of x_3^L, in the range $x_w^L \le x_3^L \le x_\pi^L$, is supposed known. The corresponding value of θ is determined by iteration. The procedure is initiated by assuming a value of $C^{LV}(0)$, say C_i^{LV}, determining the value of $x^L(0; C_i^{LV})$ from eq 21 and the value of $x^V(0; C_i^{LV})$ from eq 7. Then eqs 23−25 are numerically integrated. The integration starts where the liquid−vapor interface crosses the longitudinal axis of symmetry and continues until $y(\phi_m; C_i^{LV})$ is equal to r_{cy}. This gives ϕ_m, $x^L(\phi_m; C_i^{LV})$, and if it is different than the assumed value of x_3^L, another value of $C^{LV}(0)$ is assumed, and the process is repeated until convergence is achieved. The value of θ can be calculated from ϕ_m using eq 26.

The solid lines in Figure 2A, B were obtained for water in cylinders of different radii, each maintained at 5 °C, and rotated at the three rates indicated. In Figure 2A, the range of x_3^L values considered are those for which θ can exist. The calculations were extended over all possible contact angles, but we never observed values of θ greater than $\sim \pi/2$;[2] thus, in the following, we will confine our attention to $x_w^L \le x_3^L \le 1$.

A measurement of the meniscus height, z_m, was made in each experiment (see Tables 1 and 2). The value of θ and x_3^L corresponding to the measured value of z_m was also determined by solving eqs 21 to 27 iteratively, but in this case, the procedure was for the solution to converge to the measured value of z_m. The data points in Figure 2 were obtained by this procedure.

In Figure 2B, for each sized cylinder, the largest value of both θ and x_3^L were observed in the stationary cylinders. In the cylinders of progressively larger radii, both θ and x_3^L increased, and the increase in θ that results from an increase in the cylinder radius corresponds closely with that predicted (the solid lines). As indicated in Table 1, a similar result was observed at each temperature.

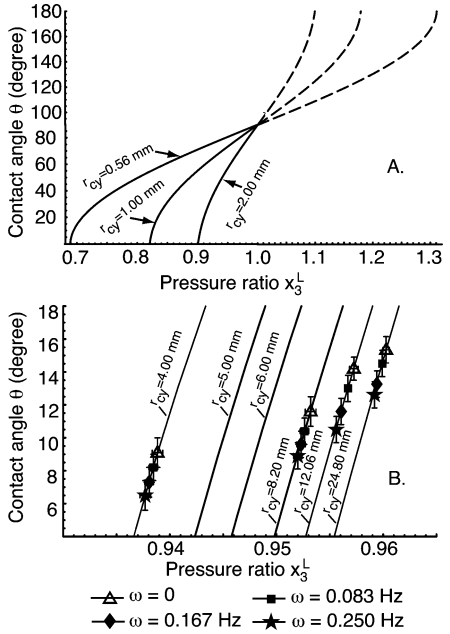

Figure 2. Contact angle dependence on pressure ratio at 5 °C. The solid lines are the predicted relation between θ and x_3^L. The data points were obtained from the measured meniscus height z_m. Note that for each sized cylinder, the largest contact angle was observed when the cylinders were stationary.

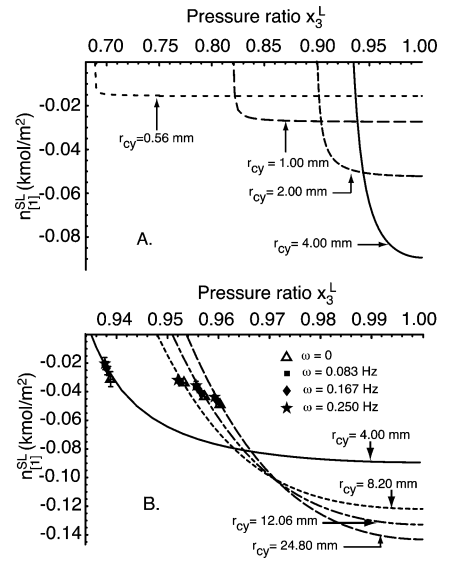

Figure 3. 5 °C adsorption isotherms of water adsorbing on borosilicate glass as a function of x_3^L.

The reason x_3^L decreased when the cylinders were rotated is discussed below. Here, we note that rotation lowered θ in each cylinder. Also, we note that the observed values of θ that were obtained by the two methods of changing x_3^L are in agreement with the predictions. In other words, the $\theta(x_3^L)$ relation is independent of how the value of x_3^L was established.

As indicated in eq 16, the value of $\gamma_{[1]}^{SL}$ may be calculated for each value of θ, and since θ may be predicted as a function of x_3^L, $\gamma_{[1]}^{SL}$ can as well. An increase in x_3^L is indicated to increase θ. This would mean $\gamma_{[1]}^{SL}$ is increased as x_3^L is increased (see eq 16).

4.1. Adsorption Isotherms at the Solid−Liquid Interface. To understand the mechanism by which x_3^L increases $\gamma_{[1]}^{SL}$ and θ, we consider the adsorption at the solid−liquid interface, $n_{[1]}^{SL}(x_3^L)$. In Figure 3, the values of $n_{[1]}^{SL}$ that are obtained from

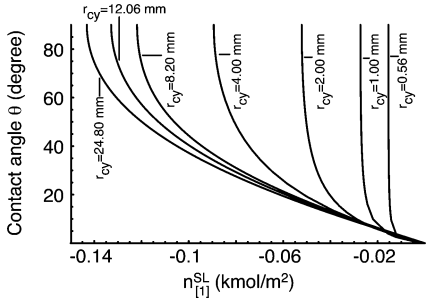

Figure 4. Contact angle of water on borosilicate glass at 5 °C as a function of the adsorption at the solid−liquid interface.

eq 18 using the relations between x_3^L and θ are shown. For those cylinders with radii of 8.20, 12.06, and 24.80 mm, third-order polynomials were used to numerically fit the relations between θ and x_3^L. The value of the correlation coefficient in the polynomial fits, R^2, in each case, was better than 0.9999. These polynomial relations were substituted into eq 18 to obtain $n_{[1]}^{SL}(x_3^L)$. However, for the cylinders with radii of 0.56, 1.00, 2.00, and 4.00 mm, a modification of this approach is needed to obtain $n_{[1]}^{SL}(x_3^L)$ values. The procedure in the previous section gives θ as a function of x_3^L, but in order to apply eq 18, the slope of $\theta(x_3^L)$ is required, and it could not be obtained with sufficient accuracy from the polynomials.

The slope was obtained by first applying the iterative procedure described in section 4 to determine the value of θ that corresponds to a x_3^L value, denoted as $\theta(x_3^L)$; second, the iterative procedure was applied again to obtain the value of θ that corresponds to $x_3^L + \delta x_3^L$, denoted as $\theta(x_3^L + \delta x_3^L)$; third, $\theta(x_3^L)$ and $\theta(x_3^L + \delta x_3^L)$ were substituted into eq 28 to obtain $\mathrm{d}\theta(x_3^L)/\mathrm{d}x_3^L$:

$$\frac{\mathrm{d}\theta(x_3^L)}{\mathrm{d}x_3^L} = \frac{\theta(x_3^L + \delta x_3^L) - \theta(x_3^L)}{\delta x_3^L} \tag{28}$$

The step in x_3^L, δx_3^L, was chosen to be 10^{-8}. Changing δx_3^L from 10^{-8} to 10^{-9} only changes $n_{[1]}^{SL}(x_3^L)$ by less than 0.06%.

The 5 °C adsorption isotherms at the solid−liquid interface that are obtained from the predicted $\theta(x_3^L)$ relation are shown as lines in Figure 3. Note that x_w^L increases with cylinder radius and that, when $x_3^L > x_w^L$, the adsorption is predicted to decrease to a negative plateau value that depends on the cylinder radius. The plateau value of $n_{[1]}^{SL}$ is sensitive to the cylinder radius for the cylinders of smaller radii (i.e., $r_{cy} \leq 4$ mm), but for the cylinders of larger radii, $n_{[1]}^{SL}$ becomes progressively less sensitive to cylinder radius.

The measured adsorption at the solid−liquid interface can be obtained by (1) applying a second-order polynomial to fit the four experimental data points in each cylinder shown in Figure 2. The correlation coefficient of the polynomial fit, R^2, is found to be better than 0.999 for each cylinder. (2) Then the polynomial relation can be used in eq 18 to obtain $(x_3^L, n_{[1]}^{SL}(x_3^L))$ for each experiment in the same cylinder. The measured values of $n_{[1]}^{SL}(x_3^L)$ obtained by this procedure are shown along with the predicted isotherms in Figure 3. As seen there, the agreement is very good, although the data is limited to a small range of x_3^L values.

4.2. Relation of the Contact Angle to the Adsorption at the Solid−Liquid Interface. The dependence of θ on $n_{[1]}^{SL}$ is illustrated in Figure 4. As seen there, for a given cylinder radius, θ increases as the adsorption becomes more negative. Once

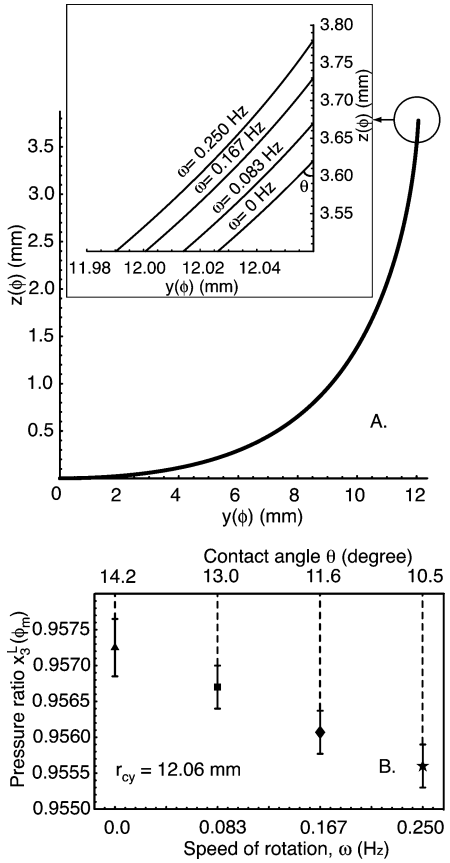

Figure 5. (A) Calculated interface shape of water held in a cylinder of 12.06 mm radius, maintained at 5 °C, while in the normal g-field, and rotated at three different rates. (B) As the rotation rate was increased, both $x_3^L(\phi_m)$ and θ decreased.

$n_{[1]}^{SL}$ has reached its plateau value, θ becomes very sensitive to any further decrease in $n_{[1]}^{SL}$. However, as seen in Figure 3 any further decrease in $n_{[1]}^{SL}$ requires a substantial increase in x_3^L. Thus, the increase in θ that results from an increase in x_3^L is caused by $n_{[1]}^{SL}$ becoming more negative. This result is examined further below when the meaning of negative adsorption is examined.

As seen in Figure 2, when the cylinders were rotated, in each case, both θ and x_3^L decreased. The reason for the decrease can be understood from the results shown in Figure 5. The upper portion of this figure indicates the calculated shape of the liquid−vapor interface, and the detail drawing near the cylinder wall indicates that the height of the three-phase line, in the gravitational field, increases with ω. This would tend to decrease x_3^L, but the centrifugal effect would tend to increase x_3^L. In the lower portion of Figure 5, the net result of the rotation is seen to be to decrease x_3^L, and the observed contact angle also decreased. The data points in Figure 5 are also shown in Figure 2 where they may be compared with the predicted relation between θ and x_3^L. Note there was no measurable disagreement between the two. Both the predicted relation of θ to x_3^L, the solid lines in Figure 2, and the experimental data indicate that, in each cylinder, θ increases as x_3^L increases. An increase in x_3^L is seen in Figure 3 to result in a decrease in $n_{[1]}^{SL}$ and is seen in Figure 4 to result in an increase in θ.

Although x_3^L is the control variable, the mechanism by which it changes θ is adsorption at the solid−liquid interface. It is important to note that an increase in x_3^L results in $n_{[1]}^{SL}$ becoming more negative, and most importantly, the experimental

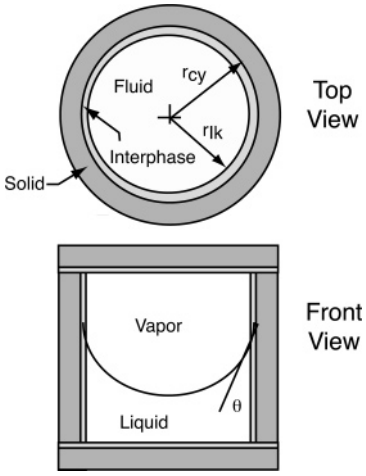

Figure 6. Schematic of the three-phase region of an axi-symmetric system.

data points are in agreement with the predicted relation between θ and x_3^L, the solid lines in Figure 2. The maximum deviation of the experimental data points from the predicted relation $\theta(x_3^L)$ is 0.2°. Thus, increasing the speed of rotation is only a means of decreasing the pressure ratio, x_3^L. Similarly, increasing the cylinder radius is only a means of increasing x_3^L.

5. Effect of Negative Adsorption on the Concentration of the Fluid Component in the Interphase

Since $n_{[1]}^{SL}[x^L(z)]$ is negative, the average concentration of the liquid component in the interphase can be shown to be less than that in the bulk. A schematic of an axi-symmetric system is shown in Figure 6. The radius r_{cyk}, where k is L or V may be taken to be the minimum radius at which the concentration of the solid component has its bulk value, n^S. At a height z, the radius of the start of the interphase region, r_{Ik}, is the maximum radius for which a fluid phase has its bulk-phase concentration, n^L or n^V, respectively. The position of the Gibbs dividing surface, at a height z, r_{dSk} has been taken to be such that there is no adsorption of the solid component. The interphase exists in the range $r_{Ik} \le r \le r_{cyk}$. The values of r_{IL} and r_{IV} would be expected to be different and to depend on height. The density of the solid component in the interphase is denoted $n^S f_{Sk}(r, z)$, where at the height z, $f_{Sk}(r, z)$ is a function of the radial position, r. Similarly, the densities of the vapor and liquid phases in the interphase are denoted $n^V f_V(r, z)$ and $n^L f_L(r, z)$, respectively.

Since the position of r_{dSk}, at the height z, is chosen to be such that there is no adsorption of the solid component, the total number of moles of this component in a segment of the interphase of height l may be written

$$2\pi l n^S \int_{r_{Ik}}^{r_{cyk}} f_{Sk}(r, z) r dr = \pi n^S l (r_{cyk}^2 - r_{dSk}^2) \qquad k = L \text{ or } V \quad (29)$$

The left side of eq 29 is the integral of the density distribution of the solid component over the interphase, and on the right-side it is the Gibbs model of the interphase. On rewriting eq 29,

$$r_{dSk}^2 = r_{cyk}^2 - 2\int_{r_{Ik}}^{r_{cyk}} f_{Sk}(r, z) r dr \quad (30)$$

The number of moles of the fluid component in each of the interphases may also be written in terms of the radial position of the Gibbs dividing surface at a solid-fluid interface:

$$2\pi l n^L \int_{r_{IL}}^{r_{cyL}} f_L(r,z) r \mathrm{d}r = \pi n^{\mathrm{L}} l (r_{\mathrm{dSL}}^2 - r_{\mathrm{IL}}^2) + 2\pi r_{\mathrm{dSL}} l n_{[1]}^{\mathrm{SL}}[x^{\mathrm{L}}(z)] \quad (31)$$

$$2\pi l n^V \int_{r_{IV}}^{r_{cyV}} f_V(r,z) r dr = \pi n^{\mathrm{V}} l (r_{\mathrm{dSV}}^2 - r_{\mathrm{IV}}^2) + 2\pi r_{\mathrm{dSV}} l n_{[1]}^{\mathrm{SV}}[x^{\mathrm{V}}(z)] \quad (32)$$

After applying eq 30 in the liquid−solid interphase, combining with eq 31 and dividing both sides by l, one finds

$$2n^L \int_{r_{IL}}^{r_{cyL}} [f_L(r,z) + f_{SL}(r,z)] r dr = n^{\mathrm{L}} (r_{\mathrm{cyL}}^2 - r_{\mathrm{IL}}^2) + 2 r_{\mathrm{dSL}} n_{[1]}^{\mathrm{SL}}[x^{\mathrm{L}}(z)] \quad (33)$$

and similarly in the solid−vapor interphase

$$2n^V \int_{r_{IV}}^{r_{cyV}} [f_V(r,z) + f_{SV}(r,z)] r dr = n^{\mathrm{V}} (r_{\mathrm{cyV}}^2 - r_{\mathrm{IV}}^2) + 2 r_{\mathrm{dSV}} n_{[1]}^{\mathrm{SV}}[x^{\mathrm{V}}(z)] \quad (34)$$

Since the densities are greater than zero, the left side of eqs 33 and 34 are positive. Thus

$$n^L (r_{cyL}^2 - r_{IL}^2) + 2 r_{dSL} n_{[1]}^{SL}[x^L(z)] > 0 \quad (35)$$

and

$$n^V (r_{cyV}^2 - r_{IV}^2) + 2 r_{dSV} n_{[1]}^{SV}[x^V(z)] > 0 \quad (36)$$

Since $n_{[1]}^{SV}$ is positive, the condition in eq 36 is satisfied by the definitions of the relative values of r_{cyV} and r_{IV}. Equation 35 can be satisfied even when $n_{[1]}^{SL}[x^L(z)] < 0$, as long as

$$n_{[1]}^{SL}[x^L(z)] > \frac{-n^L (r_{cyL}^2 - r_{\mathrm{IL}}^2)}{2 r_{dSL}} \quad (37)$$

Notice that r_{IL} and $n_{[1]}^{SL}[x^L(z)]$ are related via the density distribution functions, $f_L(r,z)$ and $f_{SL}(r,z)$ (see eq 33), but these functions remain unknown.

To understand physically what negative adsorption at the solid−liquid interface means, we introduce the spatial average of $f_L(r,z)$, denoted as $\bar{f}_L(z)$:

$$\bar{f}_L(z) \equiv \frac{2}{r_{cyL}^2 - r_{IL}^2} \int_{r_{IL}}^{r_{cyL}} f_L(r,z) r dr \quad (38)$$

From eq 33

$$\bar{f}_L(z) = 1 + \frac{2 r_{dSL} n_{[1]}^{SL}[x^L(z)]}{n^L (r_{cyL}^2 - r_{IL}^2)} - \frac{2 \int_{r_{IL}}^{r_{cyL}} f_{SL}(r,z) r dr}{r_{cyL}^2 - r_{IL}^2} \quad (39)$$

Since $n_{[1]}^{SL}[x^L(z)]$ is negative, eq 39 indicates $\bar{f}_L(z)$ is less than unity. Thus, $\bar{f}_L(z) n^L < n^L$, indicating the liquid concentration within the interphase is less than that within the bulk liquid phase when the Gibbs adsorption is negative. This prediction is consistent with the measured density of water reported by Etzler and Takei:[9−12] their studies indicate the density of water in small silica pores is less than that in the bulk density. They claim this is because the ice-like, 4-hydrogen-bonded water molecules accumulate at the solid−liquid interface. This may be the molecular mechanism that would explain why the adsorption is negative adsorption which from the thermodynamic point of view only means the density of water in the interphase is less than that in the bulk. This physical meaning of negative adsorption, for a system containing only a single fluid component, is analogous to the meaning of negative adsorption for a solute.[13] Negative adsorption in that case means the solute concentration is greater in the bulk than in the interphase, and surface tension increases as the adsorption becomes more negative.

6. Possible Effect of the Three-Phase Line Curvature on the Contact Angle Value

When the Young equation is modified to take line tension into account, it is written[21]

$$\cos\theta_R = \frac{\gamma^{SV} - \gamma^{SL}}{\gamma^{LV}} - \frac{\gamma_{lvs}}{R\gamma^{LV}} \quad (40)$$

where γ_{lvs} is the line tension, R is the radius of the three-phase contact line, and θ_R is the contact angle when the three-phase line radius is R. For larger sized droplets the line tension term becomes negligible, and eq 40 simplifies:

$$\cos\theta_\infty = \frac{\gamma^{SV} - \gamma^{SL}}{\gamma^{LV}} \quad (41)$$

From eqs 40 and 41, the line tension may be expressed

$$\cos\theta_R = \cos\theta_\infty - \frac{\gamma_{lvs}}{R\gamma^{LV}} \quad (42)$$

To determine the value of γ_{lvs}, the procedure is to place a series of differently sized droplets of a particular liquid on a solid surface, measure the radius of the three-phase contact line and θ, and use linear regression to determine γ_{lvs} from eq 42. The range of γ_{lvs} values experimentally inferred from eq 42 is 7 orders of magnitude: 10^{-5} N [21] to 10^{-12} N,[25] with some values being positive and others negative. In each of those studies, the effect of adsorption at the solid−liquid interface was neglected.

The results shown in Figure 2 do not support the proposal that θ depends on the curvature of the three-phase line. For a cylinder of radius r_{cy}, the curvature of the three-phase line is $1/r_{cy}$. Note that with the curvature of the three-phase line fixed at any one of four different values, θ was observed to change when x_3^L is changed by rotating the cylinder. This suggests that it is x_3^L that controls the value of θ, not the curvature of the three-phase line of contact.

The lines in Figure 3 were predicted assuming the line tension was zero; that is, the Young equation given in eq 1 was used, not the modified Young given eq 42, and there is no measurable difference between the predictions and the measurements. The consistency of these results suggests (by Ockham's razor) that it is not necessary to introduce line tension when defining the equilibrium conditions in three-phase systems.

Previous studies of the effect of line tension on θ have not considered the curvature of the liquid−vapor interface, its effect on x_3^L, and the resulting effect on θ, perhaps because they neglected any effects of adsorption at the solid−liquid interface. However, we note that the curvature of the liquid−vapor interface can strongly affect θ through its effect on x_3^L.

To illustrate this dependence, we consider a cylinder of sufficiently small radius, so the liquid−vapor interface may be approximated as spherical, and examine the data presented in ref 2. That data was obtained by inserting a vapor phase in a vertically oriented, "b"-shaped borosilicate-glass capillary that

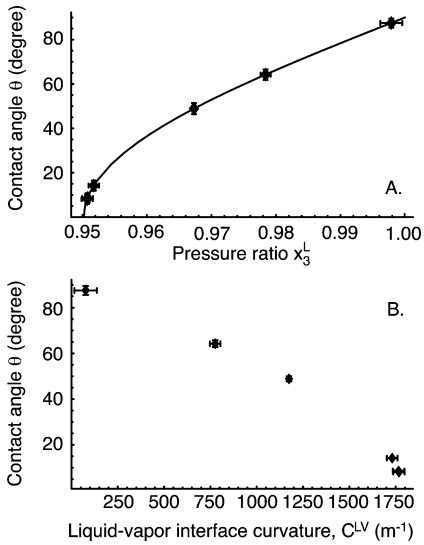

Figure 7. (A) Data points were calculated from the measured meniscus heights when water was in a 0.56 mm radius borosilicate-glass tube and maintained at 33 °C.[2] The solid line was calculated from the indicated values of x_3^L as described in section 4. (B) The value of x_3^L was used to calculate the corresponding value of the liquid−vapor interface curvature.

had Hg in the bottom portion of the b-tube but was otherwise filled with water and maintained at 33 °C. When the vapor phase was introduced and had come to equilibrium, water was both above and below the three-phase lines. In a series of experiments, the values of x_3^L at the upper and lower three-phase lines were changed by inserting vapor phases of different lengths. The meniscus heights at the three-phase lines were measured.[2]

From these measurements, the value of x_3^L and θ were determined using the procedure described in section 4. This gave the data points shown in Figure 7A. The solid line in this figure was calculated for a given value of x_3^L, also as described in section 4. Although the experimental apparatuses used to measure the meniscus heights are very different, the agreement between the predictions and the measurements seen in Figure 7A is as good as that seen in Figure 2. Note the wide range of θ and x_3^L in Figure 7A.

In the experiments of ref 2, the curvature of the liquid−vapor interface, C^{LV}, was changed as x_3^L was changed. This curvature may be calculated. When eq 19 is applied at the three-phase line and the liquid−vapor interface is spherical, one finds

$$C^{LV} = \frac{P_s}{2\gamma^{LV}}\left(\exp\left[\frac{v_f}{v_g}(x_3^L - 1)\right] - x_3^L\right) \qquad (43)$$

From the data of ref 2, the values of θ and of C^{LV} are shown in Figure 7. The results in this figure could be viewed as indicating that θ depends on C^{LV}, but eq 43 indicates that the dependence is really on x_3^L, and Figure 3 indicates that the effect of x_3^L on the adsorption at the solid−liquid interface is the mechanism by which the θ is changed when x_3^L is changed.

7. Conclusions

When the pressure is in the range where θ can exist, it was proposed that in a given system x_3^L is the independent variable of θ.[1] This proposal is supported by both series of experiments reported herein. One series used progressively larger radii borosilicate glass cylinders to increase x_3^L, and θ was observed to increase with increasing radii (see Figure 2); in the other, each cylinder was rotated at increasing rates to progressively decrease x_3^L (see Figure 5), and θ was observed to progressively decrease (see Figures 2 and 5).

The predictions (solid lines) shown in Figure 2 are only of the functional relation between θ and x_3^L. To predict the solid lines, it is only necessary to know the properties of the fluid and the cylinder radius, but to put a data point on the line, it is necessary to know the meniscus height of water in the cylinder. For a particular fluid contacting a particular solid, the meniscus height varies as x_3^L is varied. This is illustrated in Figure 2 where the meniscus height was changed by rotating the cylinders. This made the adsorption less negative (see Figure 3).

If water were put in a nonrotating cylinder of a material different than borosilicate glass, but one that had the same radius as one of the borosilicate glass cylinders and a different meniscus height was observed, then x_3^L would be different, as would $n_{[1]}^{SL}$, θ, and $\gamma_{[1]}^{SL}$. But each of these quantities can be determined by the methods discussed.

As x_3^L is increased, the adsorption at the solid−liquid interface becomes more negative (see Figure 3), and the concentration of the fluid component in the solid−liquid interphase is predicted to decrease (see eq 39). This conclusion is supported by the measurements of refs 9−12 that indicate the density of water in small diameter pores is less than the bulk density. Also, since θ is predicted to increase as x_3^L is increased, $\gamma_{[1]}^{SL}$ is also (see eqs 15 and 16). Since an increase in x_3^L makes the adsorption more negative and reduces the concentration of the liquid in the interphase, it is not surprising that $\gamma_{[1]}^{SL}$ increases as x_3^L is increased.

In formulating the conditions for equilibrium, the line tension was taken to be zero. The predictions both of θ (see Figure 7) and of the adsorption at the solid−liquid interface (see Figure 3) as a function of x_3^L were found to be in close agreement with measurements. At least for the water−borosilicate glass system, this suggests that it is unnecessary to introduce line tension in the thermodynamic description of the system. The curvature of the liquid−vapor interface does affect θ through its effect on x_3^L (see Figure 7). The curvature of the liquid−vapor interface may be the source of the droplet-size effect on contact angles that was discussed by Good and Koo.[21]

Acknowledgment. This work was supported by the Natural Sciences and Engineering Research Council of Canada.

References and Notes

(1) Ward, C. A.; Wu, J. *J. Phys. Chem.* **2007**, *111*, 3685.
(2) Wu, J.; Farouk, T.; Ward, C. A. *J. Phys. Chem.* **2007**, *111*, 6189.
(3) Rahimi, P.; Ward, C. A. *Micrograv. Sci. Technol.* **2005**, *16*, 231.
(4) Ward, C. A.; Sasges, M. R. *J. Chem. Phys.* **1998**, *109*, 3651.
(5) Sasges, M. R.; Ward, C. A. *J. Chem. Phys.* **1998**, *109*, 3661.
(6) Gibbs, J. W. *Trans. Conn. Acad. Arts Sci.* **1876**, *3*, 108; republished as *The Scientific Papers of J. Willard Gibbs*; Bumstead, H. A., Van Name, R. G., Eds.; Dover: New York, 1961; Vol. 1, p 219.
(7) Defay, R.; Prigogine, I.; Bellemans, A.; Everett, D. H. *Surface Tension and Adsorption*; Longmans, Green and Co.: London, 1966; p 24.
(8) Rowlinson, J. S.; Widon, B. *Molecular Theory of Capillarity*; Clarendon Press: Oxford, 1982; p 31.
(9) Etzler, F. M. *J. Colloid Interface Sci.* **1983**, *92*, 43.
(10) Etzler, F. M.; Fagundus, D. M. *J. Colloid Interface Sci.* **1983**, *93*, 585.
(11) Etzler, F. M.; Fagundus, D. M. *J. Colloid Interface Sci.* **1987**, *115*, 513.
(12) Takei, T.; Mukasa, K.; Kofuji, M.; Fuji, M.; Watanabe, T.; Chikazawa, M.; Kanazawa, T. *Colloid Polym. Sci.* **2000**, *278*, 475.
(13) Landau L. D.; Lifshitz, E. M. *Statistical Physics*; Pergamon Press Ltd.: London, 1958; p 465.

(14) Ward, C. A.; Rahimi, P.; Sasges, M. R.; Stanga, D. J. *Chem. Phys.* **2000**, *112*, 7195.
(15) Wensel, R. N. *Indust. Engin. Chem.* **1936**, *28*, 994.
(16) Cassie, A. B. D.; Baxter, S. *Trans. Faraday Soc.* **1944**, *40*, 546.
(17) Hiemenz, P. C. *Principles of Colloid and Surface Chemistry*; Marcel Dekker: New York, 1977; p 228.
(18) Long, J.; Chen, P. *Adv. Colloid Interface Sci.* **2006**, *127*, 55.
(19) Pease, D. C. *J. Phys. Chem.* **1945**, *49*, 107.
(20) Gao, L.; McCarthy, T. J. *Langmuir* **2007**, *23*, 3762.
(21) Good, R. J.; Koo, M. N. *J. Colloid Interface Sci.* **1979**, *7*, 283.
(22) Good, R. J. In *Surface and Colloid Science*; Good, R. J., Stromberg, R. R., Eds.; Plenum: New York, 1979; p 1.
(23) Gaydos, J.; Neumann, A. W. *J. Colloid Interface Sci.* **1987**, *120*, 76.
(24) Yekta-Fard, M.; Ponter, A. B. *J. Colloid Interface Sci.* **1988**, *126*, 134.
(25) Checco, A.; Guenoun, P.; Daillant, J. *Phys. Rev. Lett.* **2003**, *91*, 186101.
(26) Pompe, T.; Herminghaus, S. *Phys. Rev. Lett.* **2000**, *85*, 1930.
(27) Vafaei, S.; Podowski, M. Z. *Adv. Colloid Interface Sci.* **2005**, *113*, 133.
(28) Elliott, J. A. W.; Ward, C. A.; Yee, D. J. *Fluid Mech.* **1996**, *319*, 1.
(29) Münster, A. *Classical Thermodynamics*; Wiley-Interscience: Toronto, 1970; p 307.
(30) Ward, C. A.; Neumann, A. W. *J. Colloid Interface Sci.* **1974**, *49*, 286.
(31) Bashforth, F.; Adams, J. C. *An attempt to Test the Theories of Capillary Action by Comparing the Theoretical and Measured Forms of Drops*; Cambridge University Press: Cambridge, 1883.
(32) Sasges, M. R.; Ward, C. A.; Azuma, H.; Yoshihara, S. *J. Appl. Phys.* **1996**, *79*, 8770.
(33) Gibbs, J. W. *Trans. Conn. Acad. Arts Sci.* **1876**, *3*, 108; republished as *The Scientific Papers of J. Willard Gibbs*; Bumstead, H. A., Van Name, R. G., Eds.; Dover: New York, 1961; Vol. 1, p 288.